aerospace

MDPI

Article

Effect of Blade Tip Configurations on the Performance and Vibration of a Lift-Offset Coaxial Rotor

Yu-Been Lee [1] and Jae-Sang Park [2,*]

[1] Rotorcraft Flight Dynamics Team, Korea Aerospace Industries, Ltd., 78 Gongdan 1-ro, Sanam-myeon, Sacheon-si 52529, Republic of Korea
[2] Department of Aerospace Engineering, Chungnam National University, 99 Daehak-ro, Yuseong-gu, Daejeon 34134, Republic of Korea
* Correspondence: aerotor@cnu.ac.kr; Tel.: +82-42-821-6682; Fax: +82-42-825-9225

Abstract: This present study investigates the effect of blade tip configurations, such as the sweepback angle and anhedral angle, on the performance and hub vibratory loads for the lift-offset coaxial rotor of a 30,000-pound-class high-speed long-range utility helicopter. The rotorcraft comprehensive analysis code, CAMRAD II, is utilized to conduct the performance and hub vibratory load analyses for the present lift-offset coaxial rotor. The total rotor thrust, torque, and individual rotor's hub pitch moment and hub roll moment are considered the trim targets. The general properties for the lift-offset coaxial rotor are designed from the X2TD, S-97 Raider, and SB > 1 Defiant, which are lift-offset compound helicopters. The rotor performance and hub vibratory loads are studied with the various blade tip configurations including the sweepback angle and anhedral angle. The rotor power when the rotor blade tip considers only the sweepback angle (20°) is lower than the baseline rotor model by 41.25% at 170 knots. The maximum rotor effective lift-to-drag ratio (L/D_e) for the lift-offset coaxial rotor using only the sweepback angle and the rotor with both sweepback (20°) and anhedral angles (10°) at 170 knots increase by 10.82% and 5.02%, respectively, compared with the baseline rotor model without both sweepback and anhedral angles. The vibration index (VI) for the rotor with only the sweepback angle is higher than that for the baseline rotor model without both sweepback and anhedral angles by 37.14%. Furthermore, when the rotor blade tip has the anhedral angle, the magnitude of the Blade Vortex Interaction (BVI) decreases compared with the rotor without the sweepback and anhedral angles.

Keywords: lift-offset coaxial rotor (rigid coaxial rotor); performance; hub vibratory loads; sweepback angle; anhedral angle

Citation: Lee, Y.-B.; Park, J.-S. Effect of Blade Tip Configurations on the Performance and Vibration of a Lift-Offset Coaxial Rotor. *Aerospace* **2023**, *10*, 187. https://doi.org/10.3390/aerospace10020187

Received: 29 January 2023
Revised: 13 February 2023
Accepted: 14 February 2023
Published: 16 February 2023

1. Introduction

The development of high-speed long-range utility helicopters is required for the next-generation battlefields. The FLRAA (Future Long-Range Assault Aircraft) program by the United States Army, which will develop a 30,000-pound-class high-speed long-range utility helicopter to replace the UH-60 Black Hawk helicopter, is one of the representative examples [1]. Conventional helicopters with a single main rotor and tail rotor have unique flight capabilities such as vertical take-off-landing and hovering; however, they have serious problems such as slow flight speed (150–170 knots) and a short range [2]. Therefore, it is essential to develop the compound helicopter with wings or auxiliary propulsions along with the rotor, and compound helicopters with various concepts are being researched and developed extensively.

The compound helicopters using a lift-offset coaxial rotor (or rigid coaxial rotor, Figure 1) and auxiliary propulsion, among the various concepts of compound helicopters, are capable of high-speed flight over 200 knots and long-range flights as compared with conventional helicopters [3]. The lift-offset coaxial rotor with the Advancing Blade Concept (ABC) generates lift forces only on the advancing sides of the upper and lower rotors, unlike the single rotor, which generates lifts on both the advancing and retreating sides of the rotor, thus, the dynamic stall of the retreating side can be avoided at the lift-offset coaxial rotor. Furthermore, the lift-offset coaxial rotor does not need to trim the rotor hub roll moment because the hub roll moments of the upper and lower rotors are the same magnitude and in opposite directions. Thereby, the aerodynamic performance of the lift-offset coaxial rotor may be improved compared with the single rotor since more lift forces are generated on the advancing side of the lift-offset coaxial rotor. Lift-offset compound helicopters (Figure 2) appropriately reduce the rotor rotational speed and use the auxiliary propulsion system to achieve high-speed flights; however, they use blades with extremely high stiffness to maintain the spacing between the upper and lower rotor blades. Therefore, significant vibrations are generated in high-speed flights.

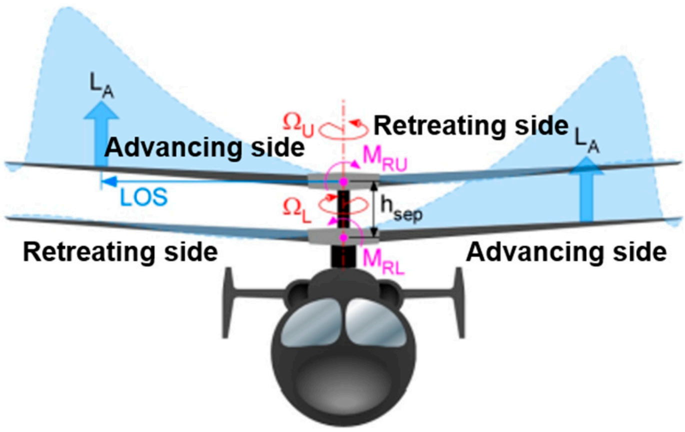

Figure 1. Lift-offset coaxial rotor [4].

Figure 2. Lift-offset compound helicopter (Sikorsky-Boeing SB > 1 Defiant).

Previous research [5–7] conducted performance and hub vibratory load analyses for the lift-offset coaxial rotors of the XH-59A and the X2 Technology Demonstrator (X2TD). The modeling and analysis techniques for the lift-offset coaxial rotor of X2TD were validated through the comparison with X2TD's flight test data [5,7]. In addition, it was shown that the rotor's effective lift-to-drag ratio (L/D_e) of the X2TD rotor with the unique design was twice as high as that of the conventional single rotor [8]. A previous study [9] used various aerodynamic models such as dynamic inflow, Viscous Vortex Particle Method (VVPM), and Computational Fluid Dynamics (CFD) for the airload analyses of the X2TD rotor.

Former studies [2,10] were also conducted on the performance and hub vibratory loads of the lift-offset coaxial rotor of the Sikorsky S-97 Raider. Furthermore, these studies also showed that the L/D_e increased when the rotor blade tip had a sweepback angle. The previous work [11] correlated the 4P hub vibratory loads between the computational fluid dynamics/computational structural dynamics coupled analyses and flight test data. Furthermore, the flight dynamics model of the S-97 Raider was developed using GenHel and compared with the flight test data [12]. The previous studies [13,14] were conducted on the wind-tunnel tests and simulation study of Sikorsky-Boeing SB > 1 Defiant (Figure 2).

The wind-tunnel test [13] was conducted with two different scale models: 1/11 scale and 1/5 scale. In particular, the 1/5 scale test studied the rotor dynamics and performance. In addition, the numerical work [14] investigated the rotor performance of SB > 1 Defiant using Sikorsky Maryland Free-Wake (SAC-MFW, [15]). However, there have not been works to study the effect of blade tip configurations, such as the sweepback angle and anhedral angle, on the performance and hub vibratory loads for the lift-offset coaxial rotor.

Therefore, this numerical study aims to predict the performance and hub vibratory loads of the lift-offset coaxial rotor of a 30,000-pound-class high-speed long-range utility helicopter using various blade tip configurations. The rotorcraft comprehensive analysis code, CAMRAD II [16], is used for the aeromechanics modeling and analyses of the present lift-offset coaxial rotor. In this work, the lift-offset coaxial rotor considers the different blade tip configurations. The first is a blade tip with the sweepback angle (Figure 3a) that improves the rotor performance [17]. The second is to consider an anhedral angle at the blade tip (Figure 3b); the anhedral angle can reduce the Blade Vortex Interaction (BVI) noise [18]. The final configuration considers both the sweepback angle and the anhedral angle at the blade tip. Thus, this paper investigates the variations in rotor power, rotor effective lift-to-drag ratio (L/D_e), and rotor hub vibration index (VI) with the different rotor blade tip configurations for the 30,000-pound-class high-speed long-range utility helicopter.

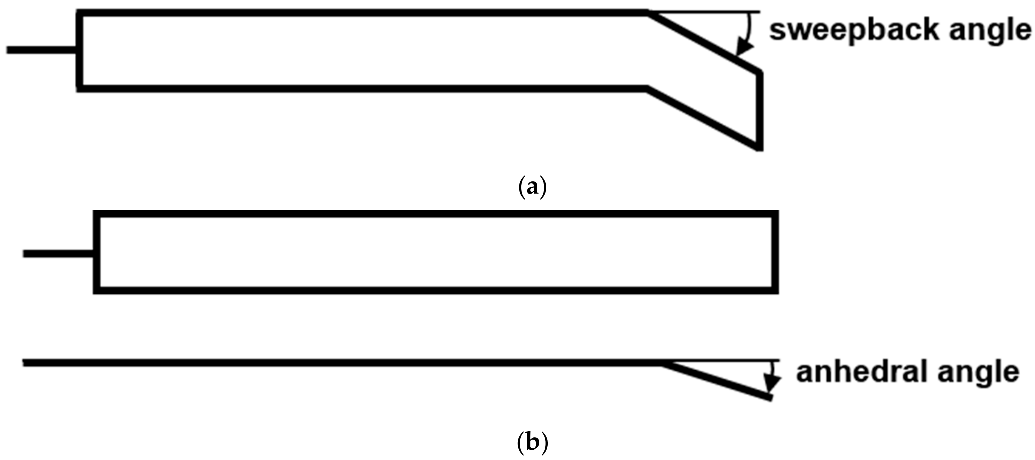

Figure 3. Various blade tip configurations [19]: (**a**) blade tip with sweepback angle; (**b**) blade tip with anhedral angle.

2. Analytical Methods

Aeromechanics Modeling and Analytical Techniques

Based on the modeling and analysis techniques using CAMRAD II for the lift-offset coaxial rotor used in the authors' previous work [7], the present lift-offset coaxial rotor for the 30,000-pound-class high-speed long-range utility helicopter is modeled and its performance and rotor vibration are investigated. In this study, four different blade tip configurations are considered for the lift-offset coaxial rotor. First, the rotor blade tip is not considered in both the sweepback angle and anhedral angle. In the second and third cases, the rotor blade tips have only the sweepback angle (20° at 90%R) or the anhedral angle (10° at 90%R). The last case uses the rotor blade tip using both the sweepback angle and the anhedral angle.

Table 1 describes the general properties of the lift-offset coaxial rotor for the 30,000-pound-class high-speed long-range utility helicopter. This hypothetical helicopter is similar to the SB > 1 Defiant helicopter with a gross weight (GW) of 30,000 lb; however, it is not designed and developed at this time. Therefore, the rotor radius is obtained from SB > 1 Defiant [20]. The blade section properties are derived and modified from those of the X2TD rotor [7] along with the application of the Mach-scaling law. In addition, the unique chord length and built-in twist distributions (Figure 4) in the radial direction are obtained from those for the lift-offset coaxial rotor model of the S-97 Raider [10]. The rotor blade has seven nonlinear finite beam elements for the blade structural dynamics modeling. The rotor control system including the swashplate, pitch link, and pitch horn is also modeled.

Table 1. General properties of 30,000-pound-class high-speed long-range utility helicopter's lift-offset coaxial rotor.

Property	Value
Gross weight, GW (lb)	30,000
Hub type	Hingeless
Number of blades per rotor	4
Rotor radius, R (ft)	25
Inter-rotor spacing, ΔZ	11.4%R
Root cutout	14.2%R
Nominal rotor speed (RPM)	249.54
Maximum flight speed (knots)	250
Coaxial rotor solidity, σ	0.1411
Cross-over angle (°)	0.0
Sweepback angle (°)	20 at 90%R
Anhedral angle (°)	10 at 90%R

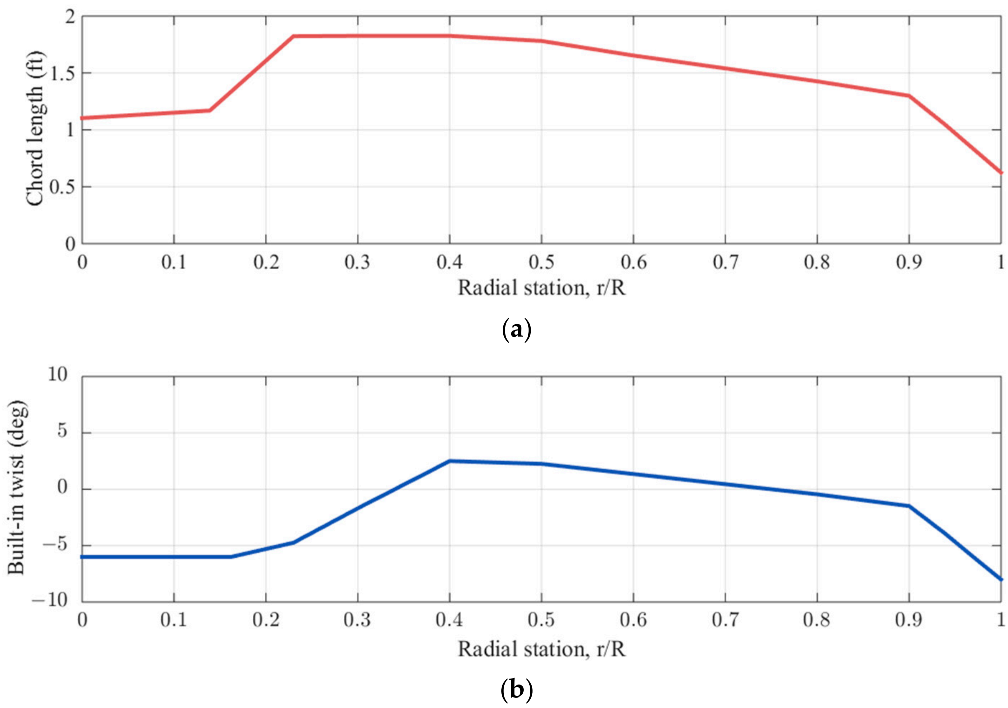

Figure 4. Chord length and built-in twist distributions: (**a**) blade chord length distribution; (**b**) blade built-in twist distribution.

The different airfoils in the radial direction (Figure 5) for the aerodynamics modeling of the lift-offset coaxial rotor are used. These airfoils are assumed identical to those of the X2TD rotor [7]. The airfoil tables including aerodynamic coefficients were generated by MSES+ [21] in the authors' previous work [7]. In addition, the Reynolds number correction method [22] is applied to the present modeling. The rotor blade consists of 25 aerodynamic panels and the width of the panels at the blade root and tip are 6.30%R and 2.60%R, respectively. Figure 6 shows the CAMRAD II model of the lift-offset coaxial rotor for the

30,000-pound-class high-speed long-range utility helicopter, particularly the rotor with only the sweepback angle.

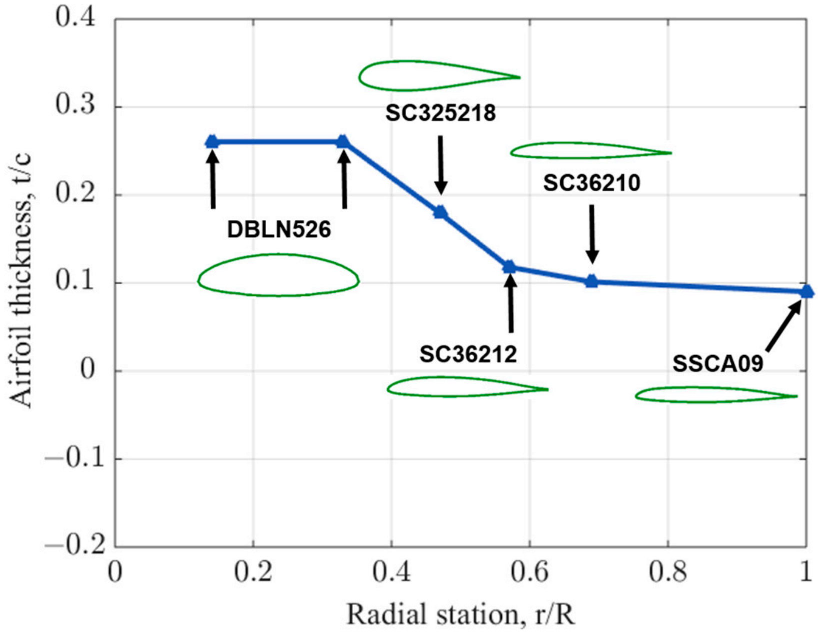

Figure 5. Airfoil section distribution.

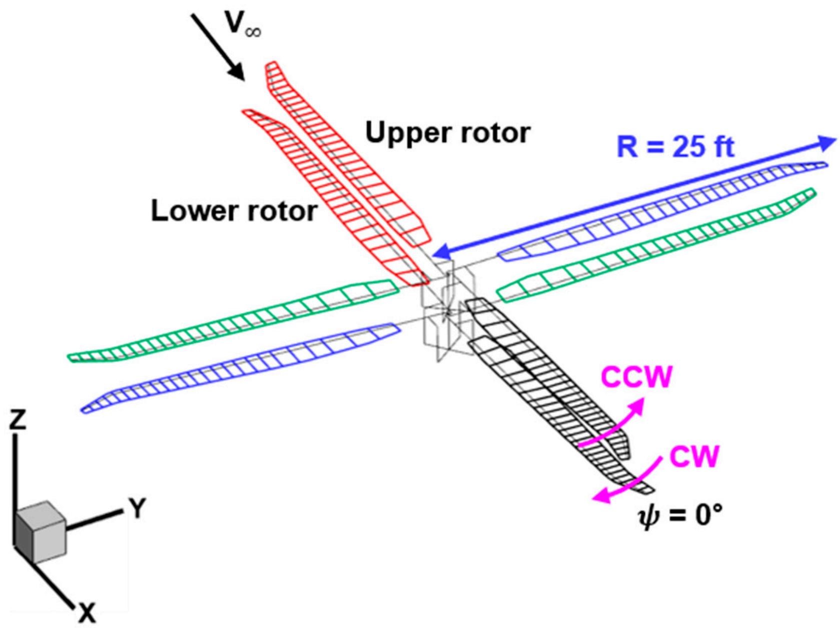

Figure 6. CAMRAD II model for lift-offset coaxial rotor with sweepback angle.

The operational and flight conditions are assumed appropriately using the results in previous studies [7,8,23] to consider the characteristics of the lift-offset coaxial rotor's performance in high-speed conditions. The rotor rotational speed decreases as the flight speed increases (87% RPM at 250 knots) to keep the Mach number at the advancing blade tip below 0.9 (Figure 7a) [8,23]. Figure 7b indicates the variation in the lift offset in terms of flight speeds. The shaft tilt angle is assumed so that the rotor power is nearly zero in high-speed flights (Figure 7c). Finally, the lift forces of the fuselage and tails (Figure 7d) are assumed as similar to the previous work [7].

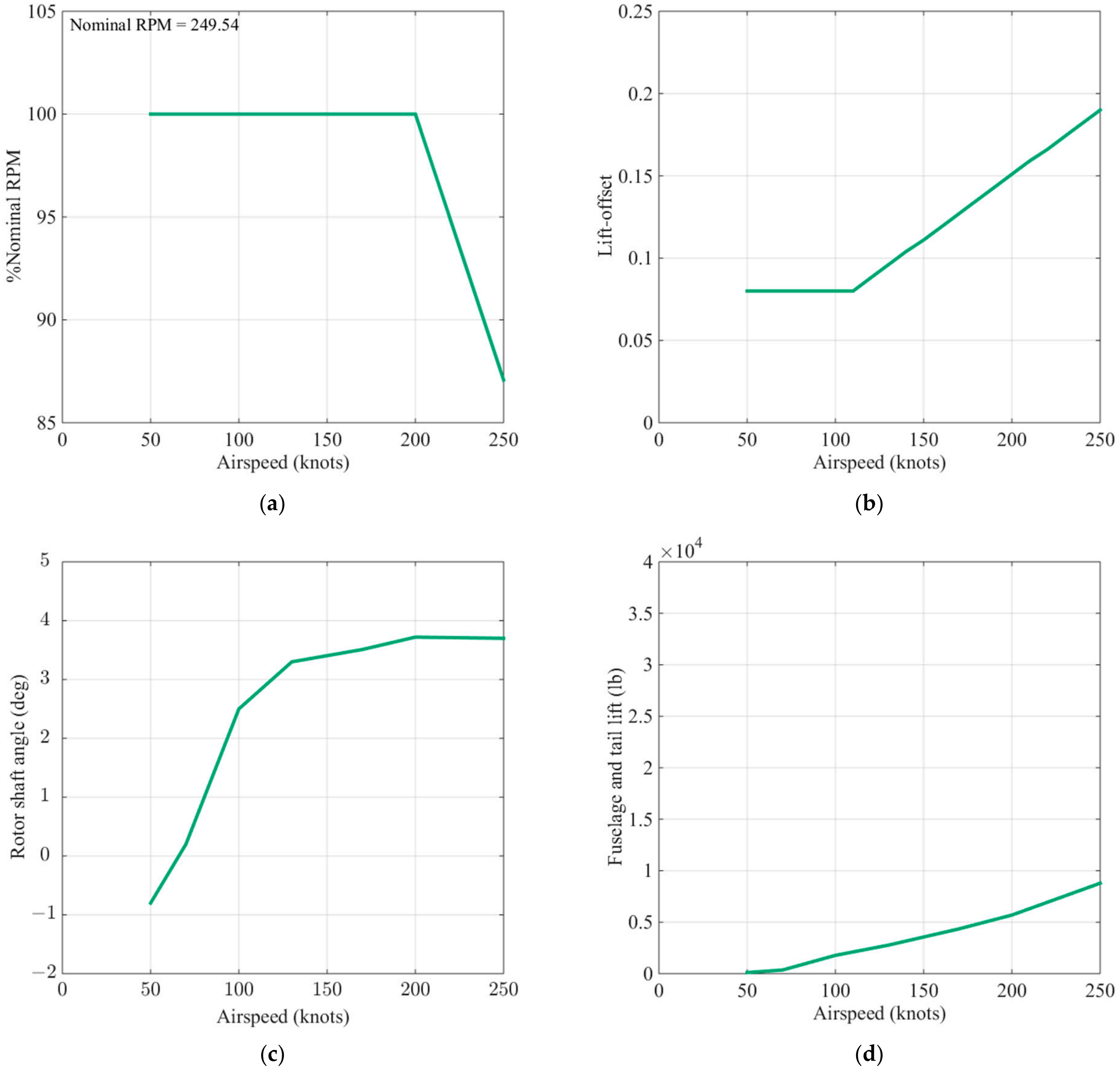

Figure 7. Operational conditions for 30,000-pound-class high-speed long-range utility helicopter: (**a**) rotor rotational speed; (**b**) lift-offset; (**c**) rotor shaft tilt angle; (**d**) fuselage and tail lifts.

The total rotor thrust, torque, and individual rotor's hub pitch moment and hub roll moment are considered as the trim targets for the present rotor. The hub roll moments (M_X) for the upper and lower rotors are calculated using the assumed lift-offset values at the given flight speeds (Figure 7b) and individual rotor's thrust (T) and rotor radius (R) using Equation (1).

$$\mathrm{LOS} = \frac{M_X}{TR} \tag{1}$$

The total rotor thrust is assumed to be the gross weight (GW = 30,000 lb) excluding the lift forces by the fuselage and tail (Figure 7d). Furthermore, the six rotor pitch control angles (θ_0^U,θ_{1c}^U,θ_{1s}^U,θ_0^L,θ_{1c}^L,θ_{1s}^L) are utilized as the trim variables. For this prediction study, the power of the pusher propeller ($P_{propeller}$) for the 30,000-pound-class high-speed long-range utility helicopter, rotor effective lift-to-drag ratio (L/D_e), and airframe drag ($D_{airframe}$) are calculated using Equations (2)–(4), respectively [7]. The propeller efficiency (η) in Equation (2) is assumed 0.85, and the total drag (D_{total}) indicates the sum of the rotor drag

(D_{rotor}) and $D_{airframe}$. The rotor vibration index (VI) is defined by Equation (5). Furthermore, the 4P hub axial force (F_{X4P}), 4P hub vertical force (F_{Z4P}), and 4P hub pitch moment (M_{Y4P}) for the total rotor only are considered in Equation (5) since the other components are canceled out by each other at the lift-offset coaxial rotor with the cross-over angle = 0° [24].

$$P_{propeller} = \frac{D_{total}V}{\eta} \tag{2}$$

$$L/D_e = \frac{L}{\frac{P_{coaxial}}{V} + D} \tag{3}$$

$$D_{airframe} = q(1.4(\frac{GW}{1000})^{\frac{2}{3}}) \tag{4}$$

$$VI = \sqrt{\frac{(0.5F_{X_{4P}})^2 + (0.67F_{Y_{4P}})^2 + (F_{Z_{4P}})^2}{GW}} + \sqrt{\frac{(M_{X_{4P}})^2 + (M_{Y_{4P}})^2}{(R)(GW)}} \tag{5}$$

In the present analyses, the rotor performance and hub vibration are calculated using an azimuthal step of 15°; however, the blade airloads are predicted with the refined azimuthal increment of 3.6° to represent elaborately the aerodynamic interference effect between the upper and lower rotors, which will be discussed in Section 3.3.

3. Results

3.1. Fan Plot Analyses

In this section, the rotating blade natural frequencies in terms of the rotor rotational speed (Figure 8) are predicted to investigate the structural dynamics of the lift-offset coaxial rotor of the 30,000-pound-class high-speed long-range utility helicopter. As shown in the figure, for the rotor blade with the sweepback angle and without the anhedral angle, the blade natural frequency in the third flap mode (F3) decreases compared with the baseline rotor model without both sweepback and anhedral angle. When the rotor blade tip considers only an anhedral angle, the blade's natural frequency in the second lead-lag mode (L2) is lower than the corresponding frequency of the baseline rotor model. Furthermore, the blade natural frequencies in the second lead-lag mode (L2) and third flap mode (F3) for the rotor model with both sweepback and anhedral angles are lower than those of the baseline rotor model. The lift-offset coaxial rotor of the 30,000-pound-class high-speed long-range utility helicopter can avoid resonance because the blade's natural frequencies do not coincide with the 4P and 8P at hover and high-speed conditions for all the blade tip configurations. In addition, it is investigated that the blade's natural frequency in the first torsion mode (T1) is higher than 10P. Therefore, the structural dynamic modeling for the 30,000-pound-class high-speed long-range utility helicopter's lift-offset coaxial rotor is built successfully using CAMRAD II.

3.2. Performance Analyses

This section analyses the rotor performances in hover and forward flights for the present 30,000-pound-class high-speed long-range utility helicopter. Figure 9 compares the Figure of Merit results in hover when two different built-in twist distributions are used. As given in the figure, since the Figure of Merit using the built-in twist distributions of an S-97 Raider (Figure 4b) is higher than when the rotor applies the built-in twist for an X2TD [4], the present lift-offset coaxial rotor model utilizes the built-in twist distributions for the S-97 Raider instead of that for the X2TD for better hover performance. Figure 10 shows the power of the 30,000-pound-class high-speed long-range utility helicopter using various blade tip configurations. As shown in the figure, for all the blade tip configurations, the rotor power decreases as the flight speed increases and becomes nearly zero in high-speed flights. In contrast, the pusher propeller power increases significantly as the flight speed increases. Therefore, it is observed that most of the power is used for driving the pusher propeller in high-speed flight. The rotor power for the rotor blade with only the sweepback angle of 20° decreases by 41.25% at 170 knots compared with the baseline rotor model (Figure 10). Thus, the sweepback angle at the blade tip can be used for the improvement of rotor performance in forward flight.

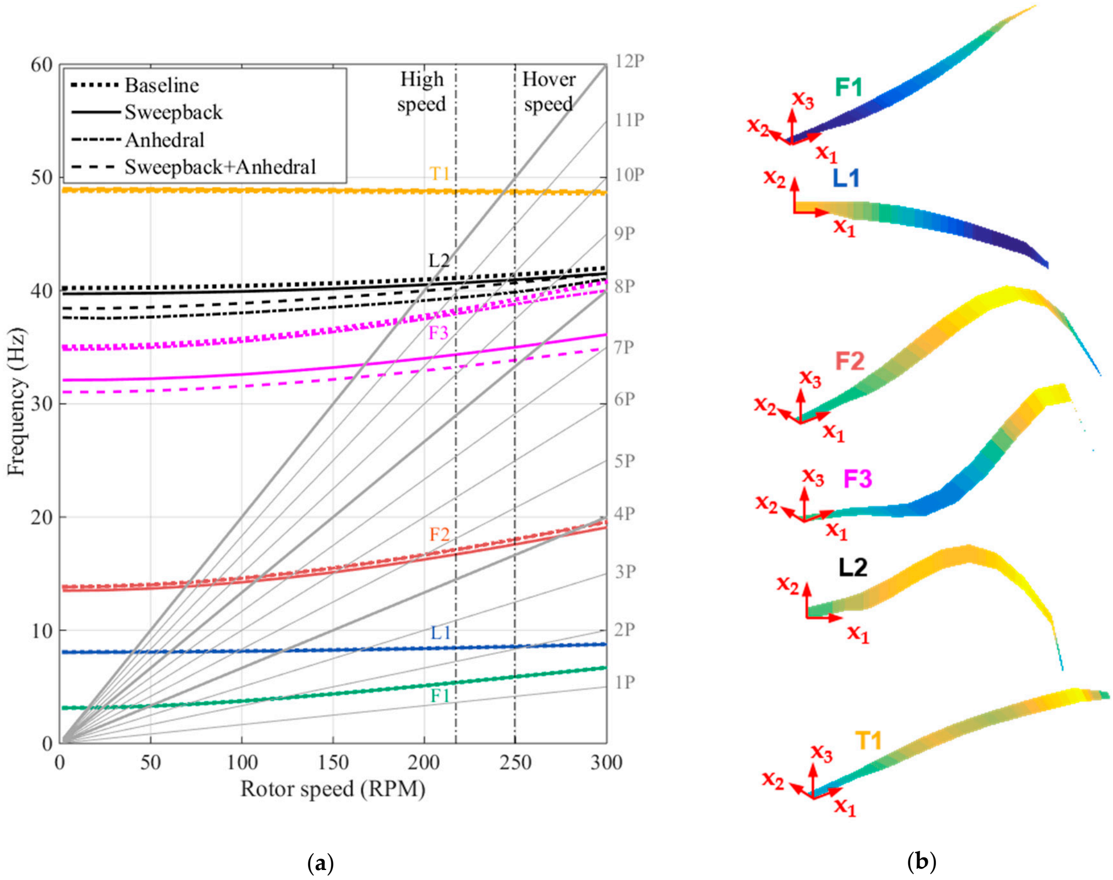

Figure 8. Natural frequencies of rotating blade for the lift-offset coaxial rotor: (**a**) rotating blade natural frequency; (**b**) mode shapes with sweepback angle at non-rotating condition.

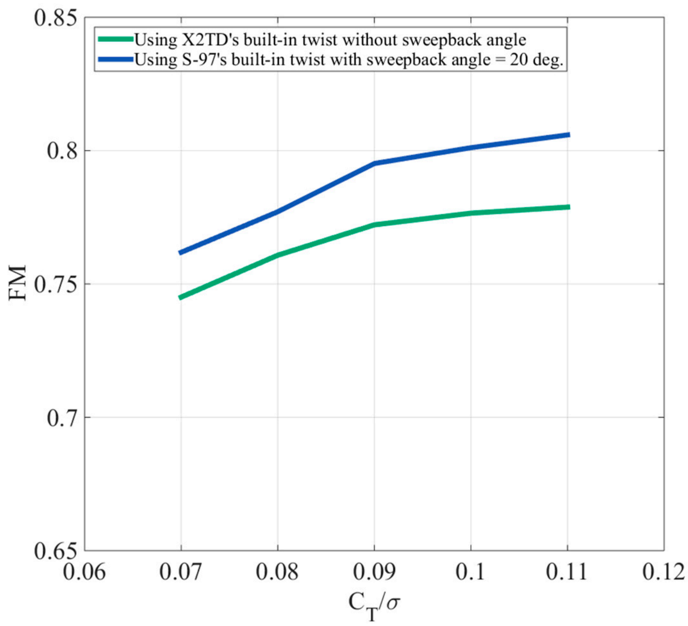

Figure 9. Figure of Merit (FM) in terms of thrust coefficient (C_T/σ).

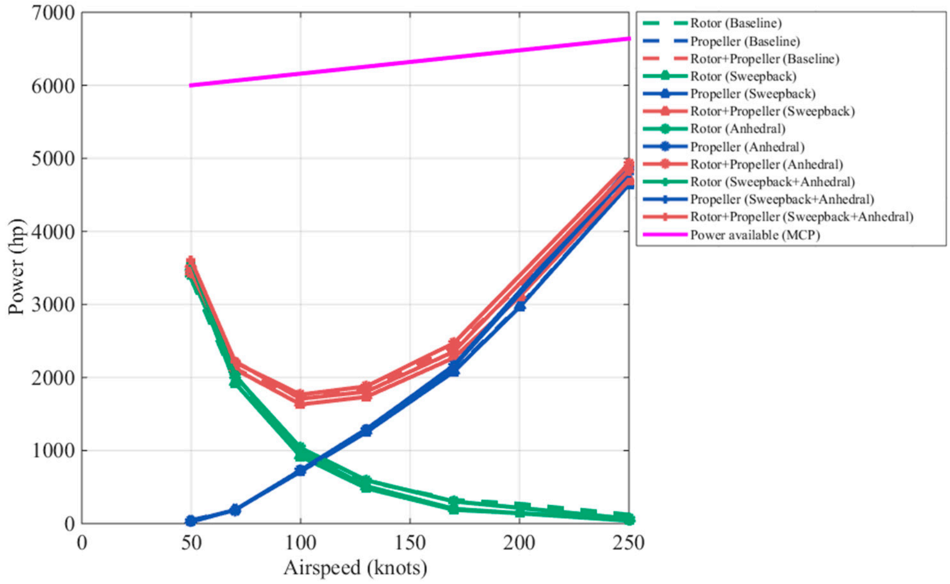

Figure 10. Power predictions in forward flight.

Figure 11 illustrates the variations in the rotor effective lift-to-drag ratio (L/D_e). The trends of L/D_e are similar for the different blade tip configurations and the L/D_e decreases with an increase in flight speed after the maximum value at 170 knots. Compared with the baseline rotor model using neither the sweepback angle nor anhedral angle, the maximum L/D_e increases by 10.82% when the rotor blade tip has a sweepback angle of 20°. The maximum L/D_e for the rotor blade with only an anhedral angle of 10° decreases by 2.75% and 12.25% at 170 knots compared with the baseline rotor model and the rotor with only a sweepback angle, respectively. In addition, when the rotor blade tip uses both sweepback and anhedral angles, the maximum L/D_e increases by 5.02% and 7.99% compared with the results for the baseline rotor model and rotor blade with only anhedral angle, respectively. Furthermore, the maximum L/D_e for the rotor blade with both sweepback and anhedral angles decreases by 5.24% as compared with that for the rotor with the sweepback angle. Thus, it is investigated that the performance of the lift-offset coaxial rotor can be improved when the rotor blade tip has a sweepback angle.

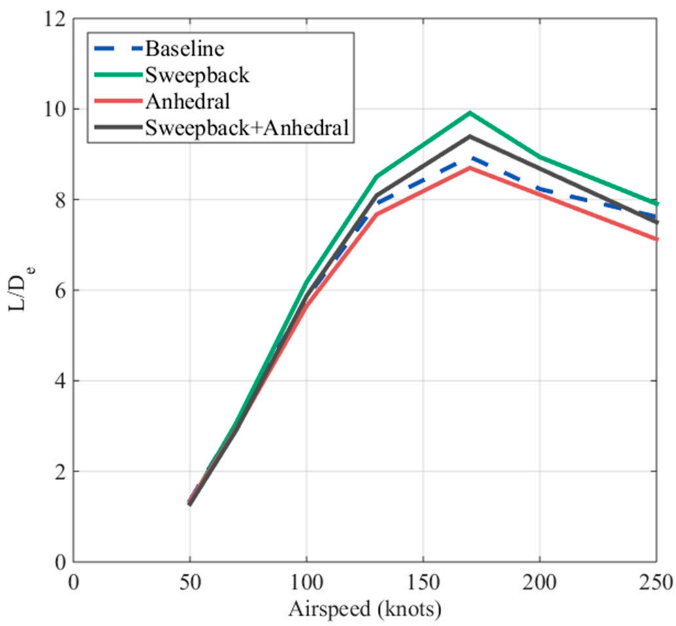

Figure 11. Rotor effective lift-to-drag ratios (L/D_e).

Figure 12 indicates the lift and drag forces for the present lift-offset coaxial rotor with both sweepback and anhedral angles, one of the various blade tip configurations. Since the variations in the lift and drag forces in terms of the airspeeds are similar for the rotors using various blade tip configurations, the results for the rotor with both sweepback and anhedral angles are described in this section. As shown in the figure, the lift forces of the upper and lower rotors are almost equal, and the lift forces for the upper and lower rotors decrease as the flight speed increases. However, the fuselage and tail lift forces increase when the flight speed increases. In addition, the drag forces for the upper and lower rotors are also similar to each other and increase with the increase in airspeed. Furthermore, the airframe drag force calculated by Equation (4) also increases as the flight speed increases.

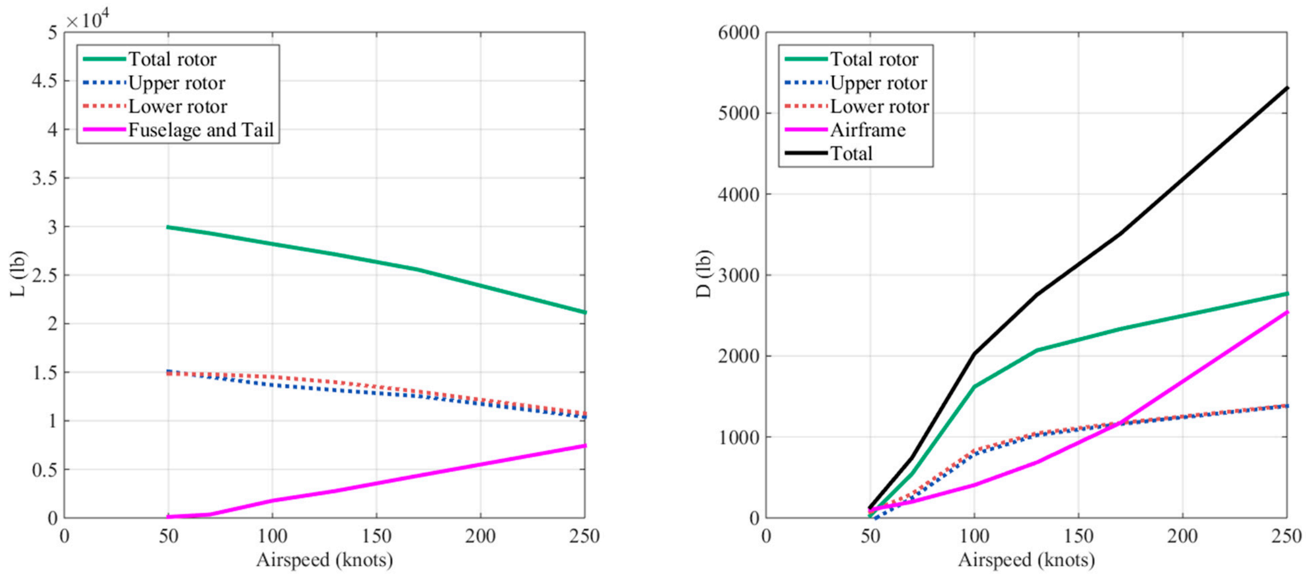

(**a**) (**b**)

Figure 12. Lift and drag forces with both sweepback and anhedral angles: (**a**) lift force (L); (**b**) drag force (D).

3.3. Blade Airload Analyses

In this section, the blade section airloads such as the lift, drag, and pitching moment at 250 knots are investigated for the lift-offset coaxial rotors with different blade tip configurations. Since the overall trends for blade airloads of rotors using various blade tip configurations are similar to each other, this section describes representatively the results for the rotor using both the sweepback and anhedral angles. The post-trim method with an azimuth angle step of 3.6° is applied to investigate elaborately the behaviors of the rotor airloads with the aerodynamic interference effect between the upper and lower rotors for the lift-offset coaxial rotor [7]. The blade section airloads are expressed using non-dimensionalized forms with the local Mach number (M). Figure 13 shows the rotor airload distributions for the baseline rotor with both sweepback and anhedral angles at 250 knots. The azimuthal angle (Ψ) in the figure is defined in the rotational direction of each rotor. As illustrated in the figure, the lift, drag, and pitching moment for the upper and lower rotors are reasonably symmetric to each other. Most lift forces are generated on the advancing side ($0° \leq \Psi \leq 180°$) for each rotor; thus, the unique characteristics of the lift-offset coaxial rotor can be clearly observed (Figure 13a). Furthermore, Figure 13a shows the negative tip loading at the blade outboard region on the advancing side and the reverse flow region on the retreating side ($180° \leq \Psi \leq 360°$). The higher drag force (Figure 13b) and positive pitching moment (Figure 13c) are shown for the blade inboard region of the upper and lower rotors on the retreating side. In addition, the highest drag is generated in the blade tip region on the advancing side due to the compressibility effect.

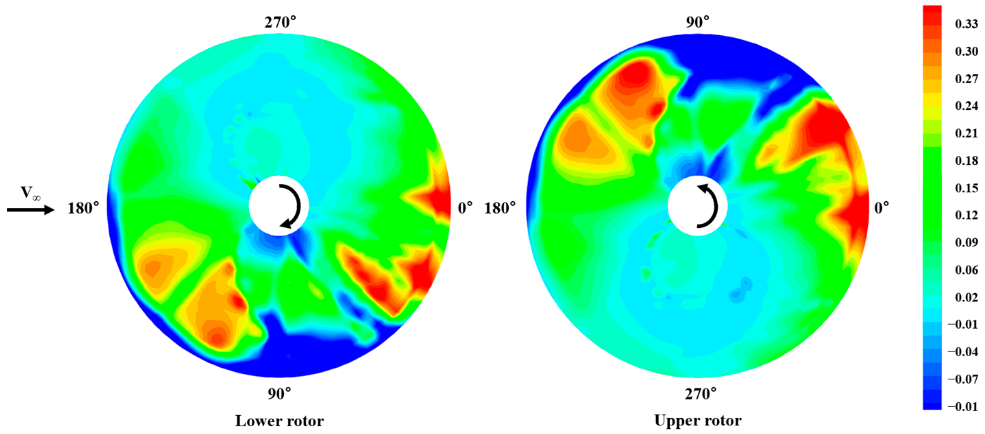

(**a**)

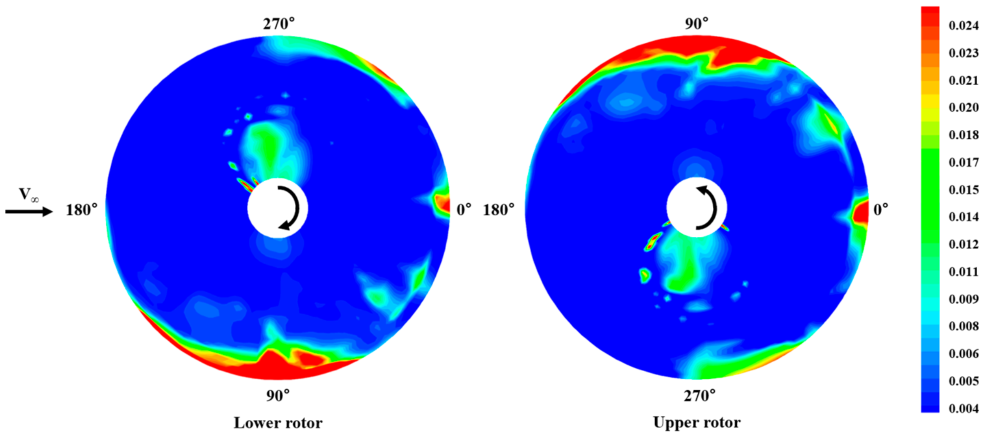

(**b**)

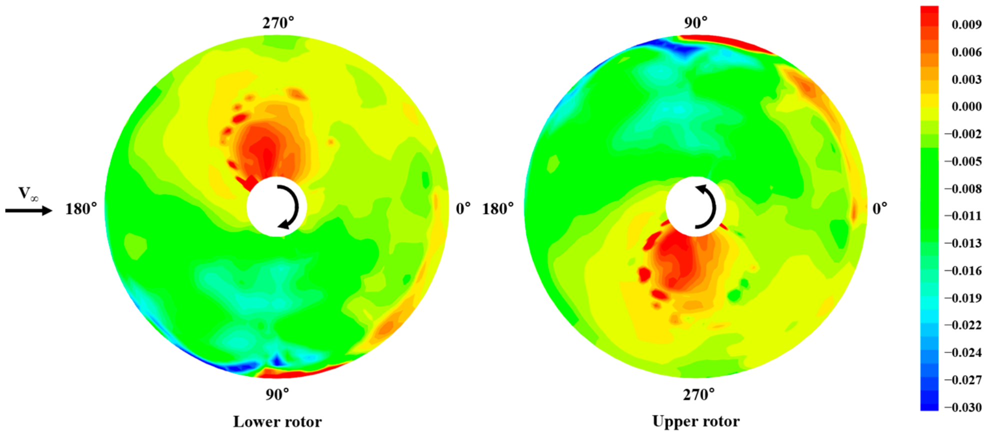

(**c**)

Figure 13. Rotor airload distributions with both sweepback and anhedral angles at 250 knots: (**a**) rotor lift force (M^2C_l); (**b**) rotor drag force (M^2C_d); (**c**) rotor pitching moment (M^2C_m).

Figures 14–17 show the blade section lift forces (M^2C_l) for one rotor revolution, using various blade tip configurations at 24%R, 55%R, and 86%R. The section lift behaviors of the upper and lower rotors are similar to each other for all the cases. The overall trends of M^2C_l in the figures are reasonably similar to each other. As previously described, most lifts are produced on the advancing side ($0° \leq \Psi \leq 180°$) of the rotor and the section lift force on the rotor retreating side ($180° \leq \Psi \leq 360°$) is nearly zero. A total of eight aerodynamic interferences between the upper and lower rotors are found for one rotor revolution. Therefore, the impulse behaviors of the section lift force due to the aerodynamic interactions are investigated at the azimuth angle interval of 45°. The M^2C_l oscillations caused by BVI are clearly investigated at $0° \leq \Psi \leq 45°$ in the blade outboard region (86%R) for both the upper and lower rotors. Furthermore, the negative section lift force is observed near the azimuth angle of 90° in the blade outboard region. Compared with the baseline rotor without both sweepback and anhedral angles, the maximum magnitude of the negative section lift forces at 86%R near Ψ = 90° increase by 64.80% and 67.61% for the rotor using only the sweepback angle and that with both sweepback and anhedral angles, respectively. The maximum negative M^2C_l at 86%R near Ψ = 90° is also higher by 24.90% for the rotor with only the anhedral angle than the result of the baseline rotor model. Therefore, the magnitudes of the negative tip loading when the rotor blade tip uses the sweepback or anhedral angle are higher than that for the baseline rotor without sweepback and anhedral angles. It is expected that the rotor vibration will increase when the rotor blade tip uses the sweepback angle, although the sweepback tip provides better aerodynamic performance (Figure 11), since the higher the negative tip loading, the more severe the rotor vibration.

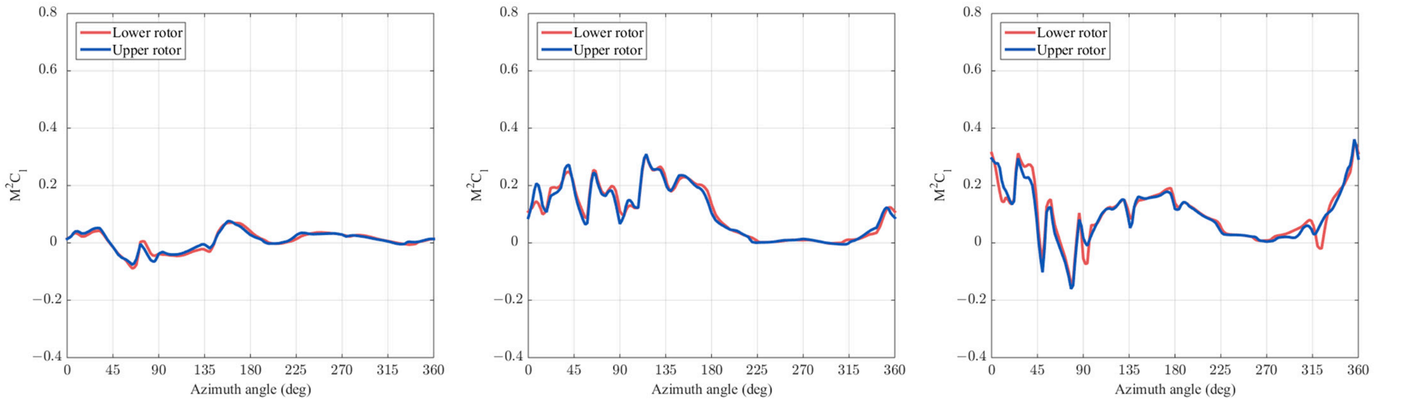

(**a**) (**b**) (**c**)

Figure 14. Rotor blade section lift force (M^2C_l) without both sweepback and anhedral angles at 250 knots: (**a**) 24%R; (**b**) 55%R; (**c**) 86%R.

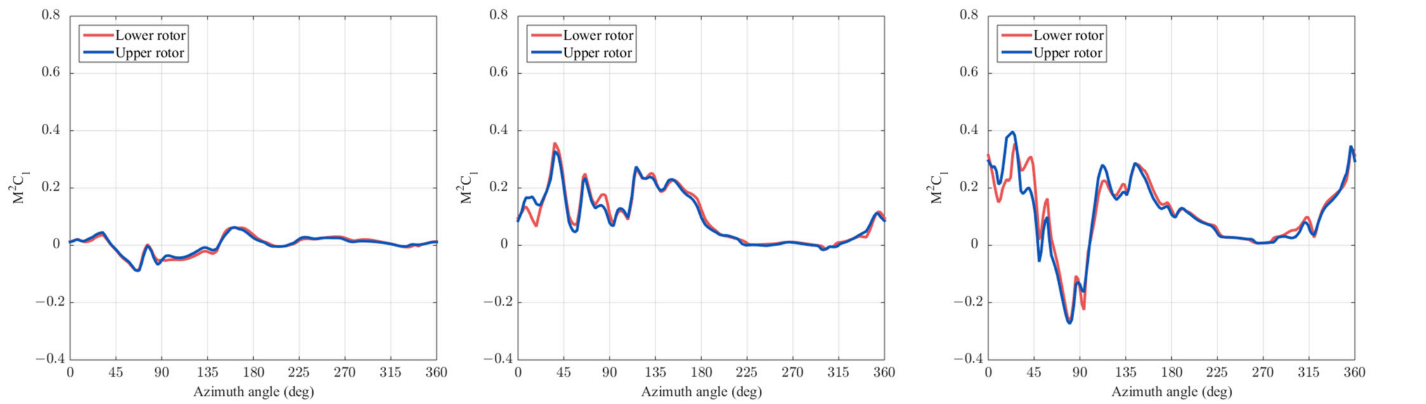

(**a**) (**b**) (**c**)

Figure 15. Rotor blade section lift force (M^2C_l) with sweepback angle and without anhedral angle at 250 knots: (**a**) 24%R; (**b**) 55%R; (**c**) 86%R.

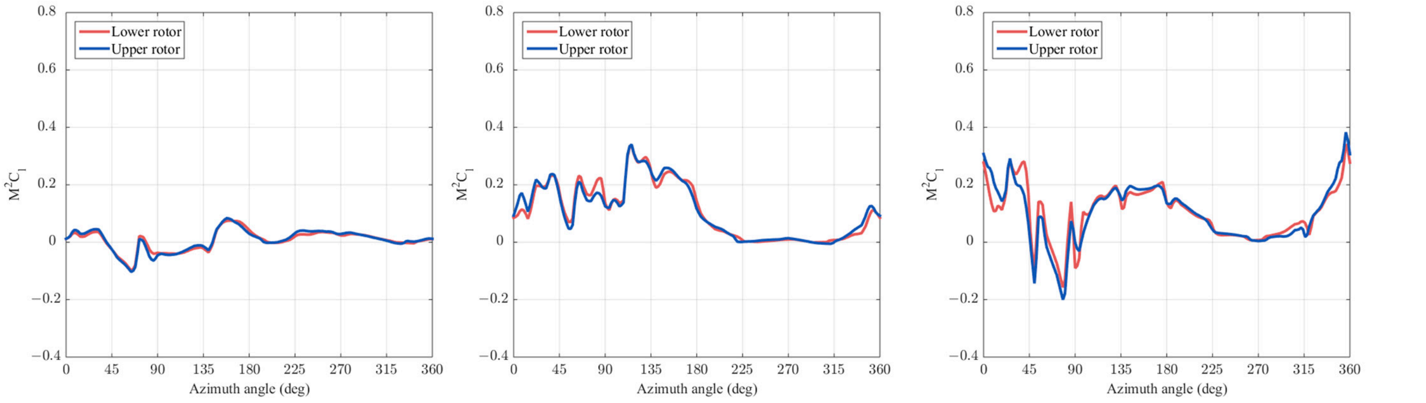

(**a**) (**b**) (**c**)

Figure 16. Rotor blade section lift force (M^2C_l) without sweepback angle and with anhedral angle at 250 knots: (**a**) 24%R; (**b**) 55%R; (**c**) 86%R.

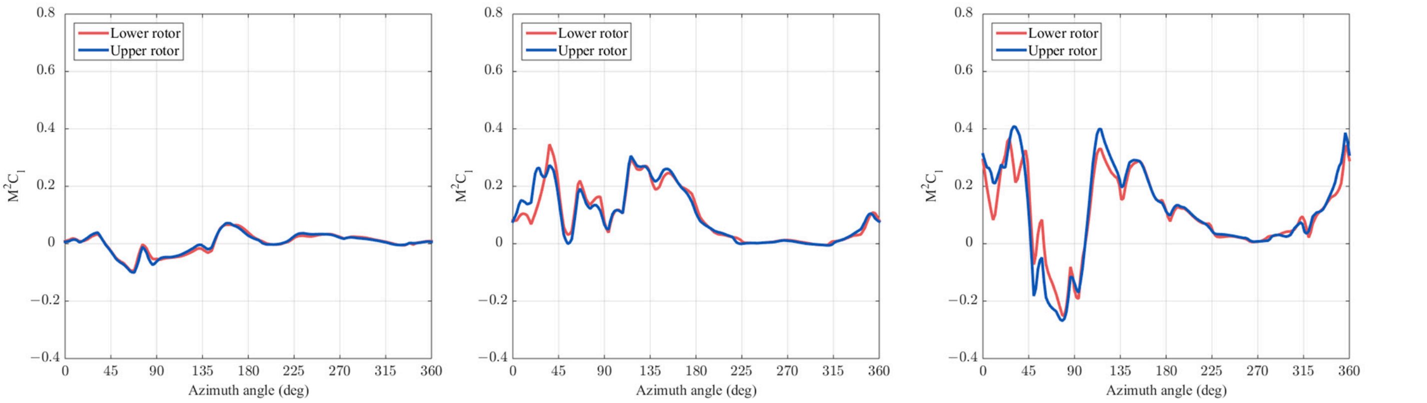

(**a**) (**b**) (**c**)

Figure 17. Rotor blade section lift force (M^2C_l) with both sweepback and anhedral angles at 250 knots: (**a**) 24%R; (**b**) 55%R; (**c**) 86%R.

The anhedral angle at the blade tip may reduce the BVI noise [18] as described previously; therefore, the section lift gradients ($d(M^2C_l)/d\Psi$) that are closely related to the rotor BVI [25,26] are investigated instead of the rotor aeroacoustics analyses in this study. In this section, Figure 18 shows the gradient of the rotor blade section lifts for the rotors using different rotor blade tip configurations. The M^2C_l gradients at $0^\circ \leq \Psi \leq 45^\circ$ in the blade outboard region where BVI is observed clearly are especially compared to investigate the effect of the anhedral angle at the rotor blade tip on the rotor BVI. The amplitudes of the rotor blade section lift gradient at $0^\circ \leq \Psi \leq 45^\circ$ with only anhedral (Figure 18b) or with both sweepback and anhedral angles (Figure 18c) decrease compared with the baseline rotor model without both sweepback and anhedral angles (Figure 18a). Therefore, it is expected that the BVI noise may be reduced when the anhedral applies at the blade tip of the lift-offset coaxial rotor.

3.4. Hub Vibratory Load Analyses

In this section, the 4P hub vibratory load variations of the lift-offset coaxial rotor are found in terms of the flight speeds for the lift-offset coaxial rotor using various blade tip configurations. As described previously, only three 4P hub vibratory load components such as the axial force (F_{X4P}), vertical force (F_{Z4P}), and pitch moment (M_{Y4P}) are considered for the total rotor when the cross-over angle = 0° is used [24]. Figure 19 shows that the 4P hub vibratory loads increase dramatically over 200 knots. Moreover, the maximum values of the 4P hub vibratory loads are found at 250 knots, which is the maximum flight speed. For the rotor with only a sweepback angle, the maximum F_{X4P} (Figure 19a) is lower by 4.43% and the maximum values of F_{Z4P} (Figure 19b) and M_{Y4P} (Figure 19c) are higher by 50.63% and 2.69%, respectively, than those for the baseline rotor without both sweepback and anhedral angles. In addition, for the rotor using only an anhedral angle, the maximum F_{Z4P} (Figure 19a) decreases by 3.06% and the maximum F_{X4P} (Figure 19b) and M_{Y4P} (Figure 19c) increase by 4.07% and 6.67%, respectively, compared with the baseline rotor model. For the rotor with the sweepback and anhedral angles, the maximum F_{X4P} (Figure 19a) is lower by 13.48% and the maximum F_{Z4P} (Figure 19b) and M_{Y4P} (Figure 19c) are higher by 43.59% and 5.98%, respectively, than those for the rotor without both sweepback and anhedral angles.

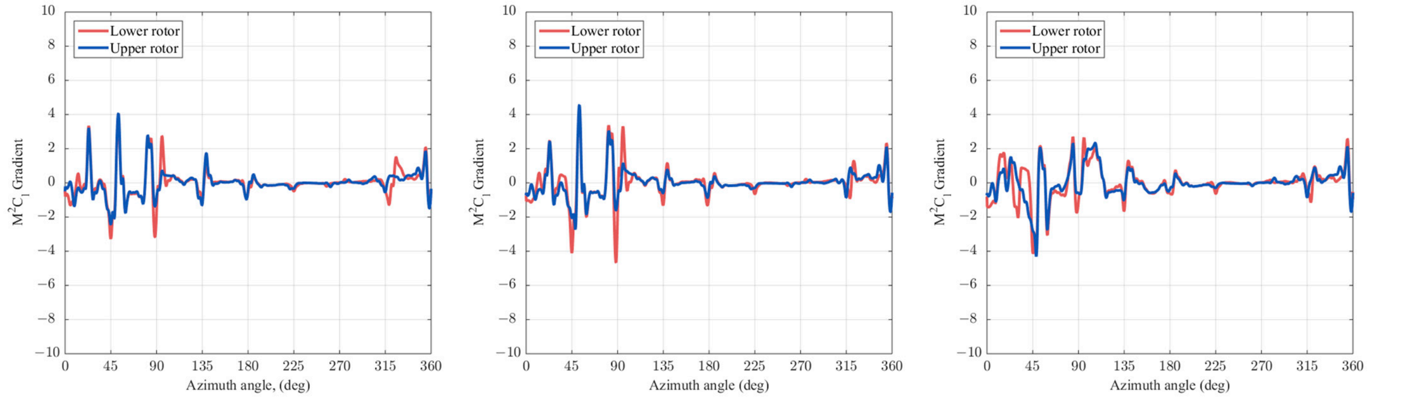

(**a**) (**b**) (**c**)

Figure 18. Rotor blade section lift force (M^2C_l) gradients in the blade outboard region (86%R) at 250 knots: (**a**) without sweepback and anhedral angles (baseline rotor model); (**b**) without sweepback and with anhedral angle; (**c**) with sweepback and anhedral angles.

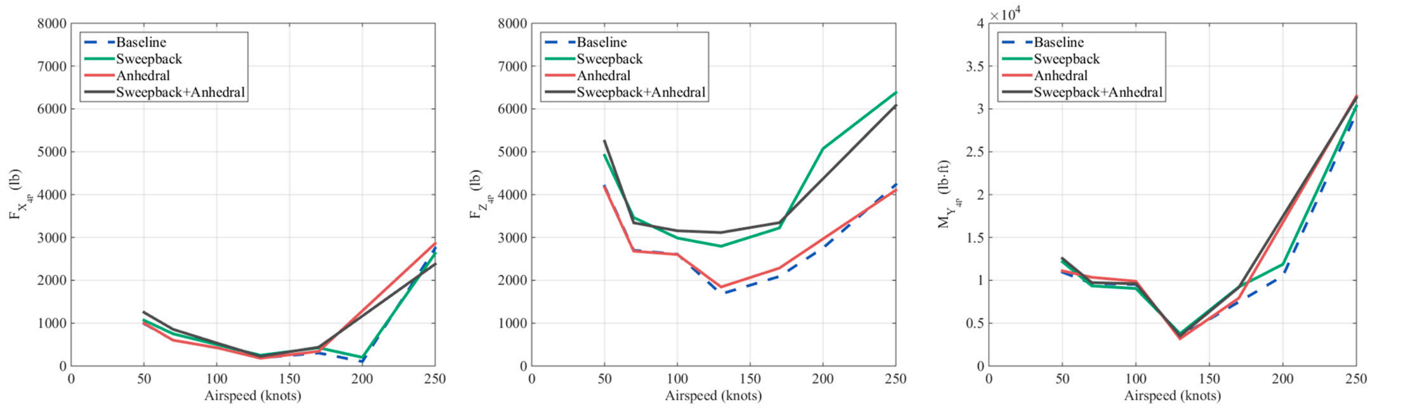

(**a**) (**b**) (**c**)

Figure 19. The 4P hub vibratory loads for the lift-offset coaxial rotor: (**a**) 4P hub axial force (F_{X4P}); (**b**) 4P hub vertical force (F_{Z4P}); (**c**) 4P hub pitch moment (M_{Y4P}).

Figure 20 indicates the rotor vibration index (VI) in terms of flight speed. The VI is calculated using Equation (5). As observed in the figure, the shapes of the VI curves for the rotors with various blade tip configurations are similar to each other. The maximum VI for the rotor with only a sweepback angle at 250 knots is higher by 37.14% than the results for the baseline rotor without sweepback and anhedral angles. It is found that the VI for the rotor with only a sweepback angle increases compared with the baseline rotor model. This is because the magnitude of the negative tip loading with the sweepback angle increases (Figures 15 and 17). The maximum values of the VI for the rotor with only an anhedral angle at 250 knots are lower by 0.47% and 27.42% than those of the baseline rotor model and the rotor with only a sweepback angle, respectively. For the rotor with both sweepback and anhedral angles, the maximum values of VI are higher by 32.20% and 32.82% than those of the baseline rotor and the rotor with only an anhedral angle, respectively. Furthermore, the maximum VI for the rotor with both sweepback and anhedral angles is lower than that for the rotor using only a sweepback angle by 3.60%. It is investigated that the sweepback angle at the rotor blade tip improves the rotor aerodynamic performance (Figure 11) but also increases the rotor hub vibration.

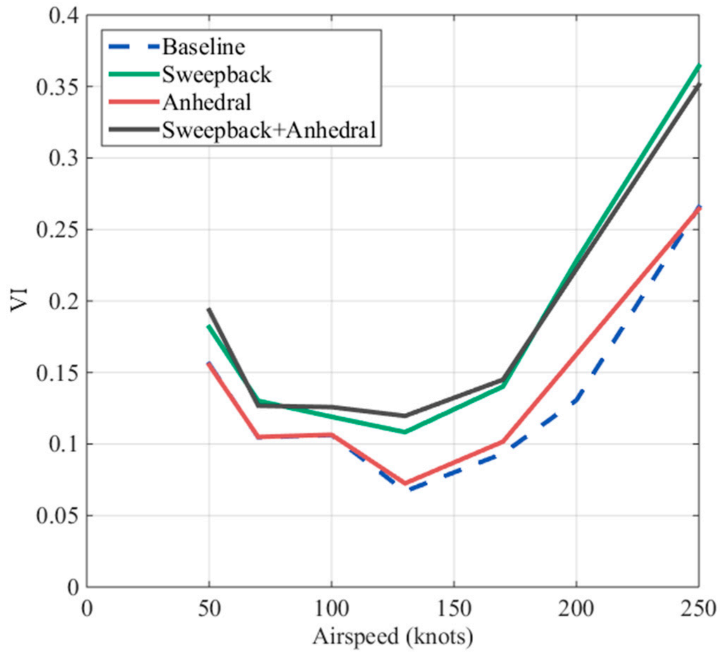

Figure 20. Rotor vibration index (VI) for the lift-offset coaxial rotor.

4. Conclusions

In this work, the performance and hub vibratory loads of the lift-offset coaxial rotor with various blade tip configurations were predicted for the 30,000-pound-class high-speed long-range utility helicopter. This present paper utilized the rotorcraft comprehensive analysis code, CAMRAD II, to investigate the performance and hub vibratory loads for the lift-offset coaxial rotor. The performance and hub vibratory loads were investigated for the lift-offset coaxial rotors with four different rotor blade tip configurations with and without sweepback and anhedral angles. The rotor power was nearly zero and the pusher propeller power increased in high-speed flights for all the blade tip configurations considered in this study. In addition, the rotor power for the rotor blade tip with only a sweepback angle was lower than the baseline rotor model at 170 knots by 41.25%. The maximum rotor effective lift-to-drag ratio (L/D_e) for the rotor using only a sweepback angle and the rotor with both sweepback and anhedral angles at 170 knots increased by 10.82% and 5.02%, respectively, compared with the baseline rotor without both sweepback and anhedral angles. Thus, this study found the lift-offset rotor performance could be improved when the rotor blade tip used the sweepback angle. This work also found variations in section lift in terms of the azimuth angle for the various rotor blade tip configurations. The Blade Vortex Interaction (BVI) in the region of $0^\circ \leq \Psi \leq 45^\circ$ at 86%R for the upper and lower rotors was observed. The magnitudes of the BVI for the rotors with only an anhedral angle and that with both sweepback and anhedral angles decreased compared with the baseline rotor model without the sweepback and anhedral angles. The present work showed that the BVI noise might be reduced for the rotor with the anhedral angle. Furthermore, the trends of the vibration index (VI) behaviors in terms of the flight speed for the rotors with various blade tip configurations were similar to each other. The VI for the rotor with only a sweepback angle was higher than that for the baseline rotor model by 37.14%. This was owing to the increase in the magnitude of the negative tip loading for the rotor with the sweepback angle. In the future, the blade design will be required for simultaneous performance improvement and vibration reduction of the lift-offset coaxial rotor.

Author Contributions: Conceptualization, J.-S.P.; methodology, J.-S.P.; software, Y.-B.L.; validation, Y.-B.L.; formal analysis, Y.-B.L.; investigation, Y.-B.L.; resources, J.-S.P.; data curation, Y.-B.L.; writing—original draft preparation, Y.-B.L.; writing—review and editing, J.-S.P.; visualization, Y.-B.L.; supervision, J.-S.P.; funding acquisition, J.-S.P. All authors have read and agreed to the published version of the manuscript.

Funding: This study was supported by Basic Science Research Program through the National Research Foundation of Korea (NRF) funded by the Ministry of Education (2020R1I1A3071793). This study was supported by the Basic Science Research Program funded by the Ministry of Science and ICT (2021R1A5A1031868). This work was supported by Korea Research Institute for defense Technology planning and advancement (KRIT) grant funded by the Korea Government (DAPA(Defense Acquisition Program Administration)) (No. KRIT-CT-22-082, Design/Manufacturing Technology of Rigid Coaxial Rotor System for High-Speed Compound Helicopter, 2023).

Institutional Review Board Statement: Not applicable.

Informed Consent Statement: Not applicable.

Data Availability Statement: The numerical data used to support the findings of this study are included within the article.

Conflicts of Interest: The authors declare no conflict of interest.

References

1. Colucci, F. The moving parts of future vertical lift. *Vertiflite* **2019**, *65*, 12–16.
2. Zhao, J.; Tuozzo, N.; Brigley, M.; Modarres, R.; Monico, M.; Makinen, S. CFD-CSD support for rotor design improvement to reduce vibrations. In Proceedings of the Vertical Flight Society (VFS) 77th Annual Forum & Technology Display, Virtual, 10–14 May 2021.
3. Ruddell, A.J.; Groth, W.; McCutcheon, R. *Advancing Blade Concept (ABC) Technology Demonstrator*; USAAVRADCOM-TR-81-D-5; Defense Technical Information Center: Fort Belvoir, VA, USA, 1981.
4. Bagai, A. Aerodynamic design of the X2 technology demonstrator^{TM} main rotor blade. In Proceedings of the 64th Annual Forum of the American Helicopter Society International, Montreal, QC, Canada, 29 April–1 May 2008.
5. Johnson, W.; Moodie, A.M.; Yeo, H. Design and performance of lift-offset rotorcraft for short-haul missions. In Proceedings of the American Helicopter Society Future Vertical Lift Aircraft Design Conference, San Francisco, CA, USA, 18–20 January 2012.
6. Go, J.-I.; Kim, D.-H.; Park, J.-S. Performance and vibration analyses of lift-offset helicopters. *Int. J. Aerosp. Eng.* **2017**, *2017*, 1865751. [CrossRef]
7. Kwon, Y.-M.; Park, J.-S.; Wie, S.-Y.; Kang, H.J.; Kim, D.-H. Aeromechanics analyses of a modern lift-offset coaxial rotor in high-speed forward flight. *Int. J. Aeronaut. Space Sci.* **2021**, *22*, 338–351. [CrossRef]
8. Walsh, D.; Weiner, S.; Arifian, K.; Lawrence, T.; Wilson, M.; Millott, T.; Blackwell, R. High airspeed testing of the Sikorsky X2 technology^{TM} demonstrator. In Proceedings of the 67th Annual Forum of the American Helicopter Society International, Virginia Beach, VA, USA, 3–5 May 2011.
9. Jacobellis, G.; Anusonti-Inthra, P.; Gandhi, F. Investigation of blade loads on a modern high-speed lift-offset coaxial helicopter using coupled computational fluid dynamics/computational structural dynamics. In Proceedings of the AHS Aeromechanics Specialists' Meeting, San Francisco, CA, USA, 16–19 January 2018.
10. Hunter, D.H.; Thomas, J.; Beatty, R.D.; Tuozzo, N.C.; Egolf, T.A.; Lorber, P.F.; Moffitt, R.C.; Westfall, S. Dual Rotor, Rotary Wing Aircraft. U.S. Patent 10822076 B2, 5 January 2021.
11. Zhao, J.; Brigley, M.; Modarres, R. S-97 Raider rotor® lower speed vibratory loads analysis using CFD-CSD. In Proceedings of the AIAA SciTech Forum, San Diego, CA, USA, 7–11 January 2019.
12. Xin, H.; Zhang, C.; Black, A.; Thorsen, A.; Luszcz, M.; Smith, T.; Herrmann, T.; Jaeger, P. S-97 Raider®GenHel model development and correlation with flight test data. In Proceedings of the Vertical Flight Society (VFS) 77th Annual Forum & Technology Display, Virtual, 10–14 May 2021.
13. Lorber, P.; Bowles, P.O.; Fox, E.; Wang, Z.K.; Hein, B.; Mayrides, B. Wind tunnel testing for the SB>1 DefiantTM joint multi-role technology demonstrator. In Proceedings of the AHS International 73rd Annual Forum & Technology Display, Fort Worth, TX, USA, 9–11 May 2017.
14. Tuozzo, N.; Fox, E.; Eller, E.; Mayrides, E.; Zientek, T.A.; Lorber, P.; Narducci, R.P.; Sproul, T. Analytical tool correlation status for the joint multi-role technology demonstrator program. In Proceedings of the AHS International 73rd Annual Forum & Technology Display, Fort Worth, TX, USA, 9–11 May 2017.
15. Bagai, A.; Leishman, J.G. Rotor free-wake modeling using a pseudoimplicit relaxation algorithm. *J. Aircr.* **1995**, *32*, 1276–1285. [CrossRef]

16. Johnson, W. *CAMRAD II: Comprehensive Analytical Model of Rotorcraft Aerodynamics and Dynamics*; Johnson Aeronautics: Palo Alto, CA, USA, 1992.
17. Desopper, A.; Lafon, P.; Philippe, J.J.; Onera, J.P. Effect of an anhedral sweptback tip on the performance of a helicopter rotor. *Vertica* **1988**, *12*, 345–355.
18. Hwang, C.; Joo, G. Parametric study for the low BVI noise rotor blade design. *Int. J. Aeronaut. Space Sci.* **2003**, *4*, 88–98. [CrossRef]
19. Kim, K.C.; Chopra, I. Aeroelastic analysis of swept, anhedral, and tapered tip rotor blades. *J. Am. Helicopter Soc.* **1992**, *37*, 15–30. [CrossRef]
20. Colucci, F. Scaling up success—Sikorsky-Boeing SB>1 Defiant. *Vertiflite* **2016**, *62*, 40–43.
21. Drela, M. *A User's Guide to MSES 3.05*; MIT Department of Aeronautics and Astronautics: Cambridge, MA, USA, 2007.
22. Lim, J.W.; McAlister, K.W.; Johnson, W. Hover Performance Correlation for Full-Scale and Model-Scale Coaxial Rotors. *J. Am. Helicopter Soc.* **2009**, *54*, 32005. [CrossRef]
23. Saberi, H.; Khoshlahjeh, M.; Ormiston, R.A.; Rutkowski, M.J. Overview of RCAS and application to advanced rotorcraft problems. In Proceedings of the AHS 4th Decennial Specialist's Conference on Aeromechanics, San Francisco, CA, USA, 21–23 January 2004.
24. O'Leary, J.; Miao, W. Design of higher harmonic control for the ABC^{TM}. *J. Am. Helicopter Soc.* **1982**, *27*, 52–57. [CrossRef]
25. Van der Wall, B.G.; Yin, J. DLR's S4 rotor code validation with HART II data: The baseline case. In Proceedings of the International Forum on Rotorcraft Multidisciplinary Technology, Seoul, Republic of Korea, 15–17 October 2007.
26. Park, J.-S.; Jung, S.N.; Park, S.-H.; Yu, Y.H. Correlation study of a rotor in descending flight using DYMORE with a freewake model. *J. Mech. Sci. Technol.* **2010**, *24*, 1583–1594. [CrossRef]